LIMNOLOGY AND OCEANOGRAPHY
Letters

ASLO
Open Access

Limnology and Oceanography Letters 9, 2024, 276–285

doi: 10.1002/lol2.10374

LETTER

Enhanced stream greenhouse gas emissions at night and during flood events

Rebecca L. Woodrow,[1]* *Shane A. White*,[1] *Stephen R. Conrad*,[1] *Praktan D. Wadnerkar*,[1] *Gerard Rocher-Ros*,[2,3] *Christian J. Sanders*,[1] *Ceylena J. Holloway*,[1] *Isaac R. Santos*[1,4]

[1]National Marine Science Centre, Southern Cross University, Coffs Harbour, New South Wales, Australia; [2]Department of Forest Ecology and Management, Swedish University of Agricultural Sciences, Uppsala, Sweden; [3]Integrative Freshwater Ecology Group, Centre for Advanced Studies of Blanes (CEAB-CSIC), Spain; [4]Department of Marine Sciences, University of Gothenburg, Gothenburg, Sweden

Scientific Significance Statement

Headwater streams release large amounts of greenhouse gases into the atmosphere. However, current global and local estimates of emissions have large uncertainties due to data scarcity, particularly during nighttime, adverse weather conditions, and in warm climates. The development of new technologies now enables detailed observations. We performed continuous, high-temporal resolution observations of dissolved nitrous oxide, methane, and carbon dioxide in a headwater stream. Increased greenhouse gas emissions at night and during heavy rainfall imply that earlier stream observations may have underestimated methane and nitrous oxide emissions by ~ 20–40% from headwater streams to the atmosphere.

Abstract

Headwater streams play a large role in aquatic greenhouse gas emissions. Carbon dioxide (CO_2) and dissolved oxygen in streams often undergo changes through diel cycles. However, methane (CH_4) and nitrous oxide (N_2O) have unknown diel dynamics. Here, we reveal consistent patterns in CO_2, CH_4, and N_2O over diel cycles and during flood events using high-frequency continuous observations in a subtropical headwater stream. Diel cycles were most pronounced during baseflow. Increased nighttime discharge due to higher groundwater inputs enhanced gas transfer velocities and concentrations. Overall nocturnal emissions were 31%, 68%, and 32% greater than daytime for CO_2, CH_4, and N_2O, respectively. Floods dampened diel signals. If both flood events and diel patterns are neglected, estimates of greenhouse gas emissions from headwaters may be greatly underestimated. Overall, CH_4 and N_2O emissions from headwater streams may be underestimated by ~ 20–40% due to a lack of observations during nighttime, floods, and in warmer climates.

*Correspondence: r.woodrow.11@student.scu.edu.au

Associate editor: John Anderson

Author Contribution Statement: RW led the manuscript effort with close support from IRS. RW, SW, and IRS conceived the idea and designed the study. SW, RW, and SC conducted fieldwork. RW and CH conducted the analysis. GR made Figs. 1–3. RW wrote the first draft. All authors contributed to the writing and editing of the manuscript.

Data Availability Statement: Data are available on https://doi.org/10.6084/m9.figshare.24439210.v1.

Additional Supporting Information may be found in the online version of this article.

Headwater streams are biogeochemical hotspots and play a major role in global riverine greenhouse gas budgets (Li et al. 2021; Marzadri et al. 2021). Estimates based on traditional discrete samples suggest that headwater streams (Strahler stream orders 1–3) contribute about 75% of global riverine CO_2, CH_4, and N_2O CO_2-equivalent (CO_2-eq) emissions (Li et al. 2021). Because they are often difficult to access and their abundance increases with decreasing stream order, the global significance of headwater streams has been difficult to quantify (Noto et al. 2022). Accurate estimates of stream fluxes are needed to reduce uncertainty in regional and global extrapolations. Large uncertainties in global summaries and models (e.g., Rocher-Ros et al. 2023; Stanley et al. 2023) in streams remain due to scarcity of measurements, geographical bias against warm climates, and a lack of high temporal resolution observations covering extreme hydrological events and diel cycles.

Stream waters reflect hydrological inputs with different biogeochemical and spatiotemporal dynamics. Stream morphology, precipitation event intensity, and surrounding ecosystems all affect greenhouse gas dynamics in headwaters (Rocher-Ros et al. 2023). Anthropogenic nitrogen and carbon inputs often enhance instream greenhouse gases (Andrews et al. 2021; Ho et al. 2022). Storms mobilize and transfer significant loads of C and N from catchment soils to headwater streams (White et al. 2021*a*) and increase downstream aquatic N_2O emissions (Woodrow et al. 2022). With climate change enhancing intense rainfall events in the subtropics (Clarke et al. 2022) and increasing agricultural and urban development, stream greenhouse gas emissions will remain difficult to predict (Yao et al. 2019; Battin et al. 2023; Rocher-Ros et al. 2023).

Stream greenhouse gas observations often rely on discrete sampling during daylight hours; however, nighttime gas dynamics can be fundamentally different than during the day. Metabolic processes such as gross primary production and ecosystem respiration are driven by day–night cycles and have a strong direct control on dissolved oxygen (DO) and CO_2 dynamics (Odum 1956; Gómez-Gener et al. 2021). Evapotranspiration may also be lower at night, raising the water table and enhancing groundwater discharge (Hill 2019). Groundwater inputs are important greenhouse gas, carbon, and nutrient sources in headwater streams (Hotchkiss et al. 2015; Lupon et al. 2019). Thus, greater groundwater connectivity can enhance gas transfer to the atmosphere. Consistently high nighttime emissions have been shown to be important for global estimates of river CO_2 emissions (Gómez-Gener et al. 2021), but little is known on diel patterns and magnitude of nighttime N_2O and CH_4 emissions.

Here, we hypothesize that diel cycles of oxygen, groundwater discharge, and terrestrial connectivity will enhance nocturnal emissions of CH_4 and N_2O. To overcome sampling bias against storm events and nighttime, we performed high temporal resolution observations of dissolved stream CO_2, CH_4, and N_2O across diel cycles and during major rainfall events in a subtropical headwater stream. We build on the literature by (1) assessing drivers of greenhouse gases over diel and hydrological cycles, (2) focusing on less studied subtropical systems with high nitrate loads that may modify greenhouse gas production, and (3) contrasting the potential climate implications of stream CO_2, CH_4, and N_2O emissions.

Methods

High-resolution temporal measurements (1 h) were performed to cover variability both on diel time scales and under contrasting hydrological conditions between 06 February and

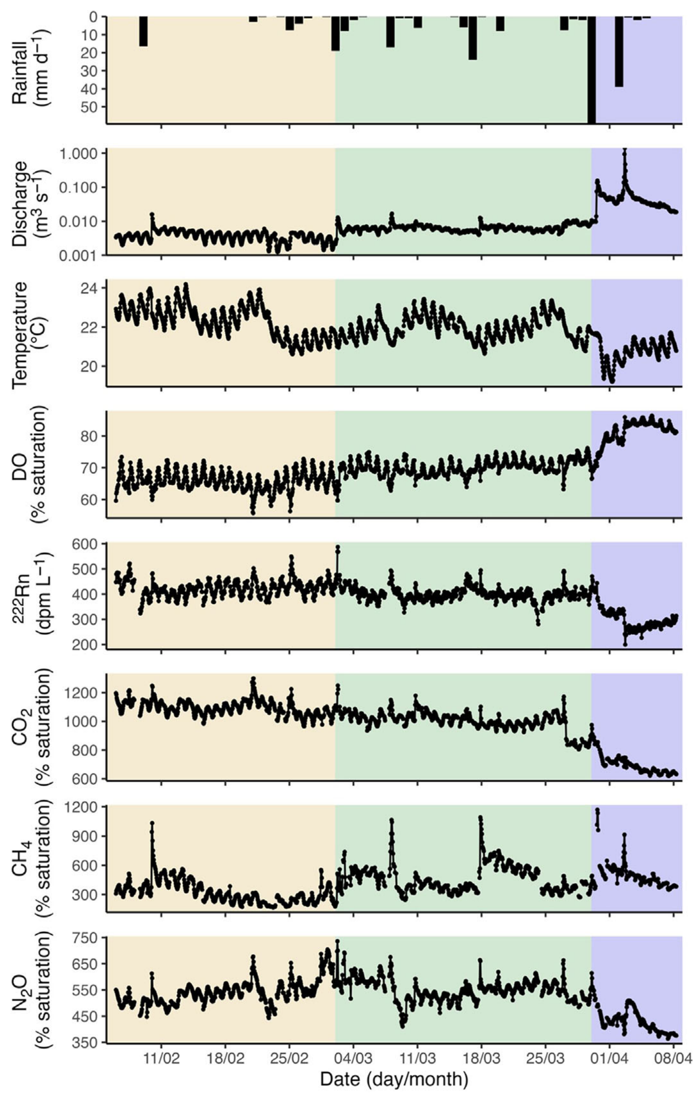

Fig. 1. Time series of hydrological and chemical parameters over 62 d of continuous observations in Double Crossing Creek capturing contrasting hydrological conditions and day–night cycles. Orange, green, and blue shading indicate periods of dry, wet, and flood, respectively.

08 April 2019 (62 d) in the subtropical catchment of Double Crossing Creek, Australia (Supporting Information Fig. S1). The average annual rainfall is 1685 mm, with ~ 40% falling between February and April (Australian Government Bureau of Meteorology 2022) (Supporting Information Fig. S2). The catchment is comprised of intensive arable horticulture (60%) with large nutrient amendments. Stream flows in this subtropical region are dominated by episodic rain events (White et al. 2021*b*) rather than seasonal cycles as in most temperate regions. Our 62 d of observations capture regional hydrological extremes, and the multiple diel cycles provide replication to day–night comparisons.

DO, pH, temperature, salinity, electrical conductivity (EC), depth, current velocity, the natural groundwater tracer radon (^{222}Rn), and the greenhouse gases N_2O, CH_4, and CO_2 were measured with a wide array of sensors and data stored using automated dataloggers, along with discrete measurements of dissolved organic carbon (DOC), nitrate (NO_3^-), and ammonium (NH_4^-) reported in a companion manuscript (White et al. 2021*a*) as explained in Supporting Information Material. Two widely used models specific to small streams (similar to our study site conditions) were used to calculate gas transfer velocities (k_{600}, m d^{-1}) and estimate water–air fluxes. The Li et al. (2019) model used chamber incubations from 30 rivers, while the Raymond et al. (2012) model was derived from metadata of direct gas tracer release experiments from > 100 rivers.

The k_{600} values were then normalized to gas-specific k values and water temperature using equations for the kinematic viscosity of water (Siedler and Peters 1986) and the

Table 1. Mean values with standard deviation and value range for water parameters, transfer velocities, and vertical fluxes over dry ($n = 24$ d, accumulated rainfall 33 mm), wet ($n = 28$ d, accumulated rainfall 104 mm), and flood ($n = 10$ d, accumulated rainfall 102 mm) conditions in Double Crossing Creek, Australia.

		Dry		Wet		Flood	
Parameter	**Units**	**Mean±SD**	**Range**	**Mean±SD**	**Range**	**Mean±SD**	**Range**
Current velocity	m s^{-1}	0.22±0.04	0.14–0.57	0.29±0.04	0–0.59	0.42±0.01	0.21–1.43
Depth	m	0.08±0.01	0.043–0.14	0.11±0.01	0.064–0.142	0.18±0.03	0.121–0.31
Discharge	m^3 s^{-1}	0.004±0.001	0.001–0.02	0.01±0.04	0.002–0.02	0.06±0.12	0.011–1.42
Slope				0.00492			
Gas concentration							
CO_2	% sat.	1085±52	957–1295	996±64	798–1230	691±4765	614–967
CH_4	% sat.	324±117	169–1037	463±143	287–358	500±121	351–476
N_2O	% sat.	534±45	439–698	543±43	480–492	429±47	366–385
Gas transfer velocity(k_{600})							
Raymond et al. (2012)							
CO_2	m d^{-1}	3.3±0.9	1.5–9.9	4.6±0.7	2.1–9.9	8.3±4.1	4–33.2
CH_4	m d^{-1}	3.2±0.9	1.5–9.8	4.5±0.7	2.1–9.8	8.2±4.1	4–32.7
N_2O	m d^{-1}	3.2±0.9	1.5–9.9	4.6±0.7	2.1–9.8	8.2±4.1	4–32.7
Vertical flux from k_{600}							
Raymond et al. (2012)							
CO_2	mmol m^{-2} d^{-1}	471±141	201–1655	616±130	320.3–1507	756±425	324.2–3153
CH_4	mmol m^{-2} d^{-1}	0.02±0.02	0–0.2	0.05±0.03	0.01–0.25	0.1±0.1	0.03–0.7
N_2O	μmol m^{-2} d^{-1}	123±36	47–435	181±39	90.4–458	255±144	100.7–862.4
Gas transfer velocity (k_{600})							
Li et al. (2019)							
CO_2	m d^{-1}	5.3±0.7	3.96–10.9	6.3±0.6	4.34–10.8	8.1±2.9	4.94–23.7
CH_4	m d^{-1}	5.2±0.7	3.91–10.7	6.2±0.6	4.28–10.7	8±2.9	4.87–23.4
N_2O	m d^{-1}	5.3±0.7	3.94–10.8	6.3±0.6	4.32–10.8	8.1±2.9	4.91–23.6
Vertical flux from k_{600}							
Li et al. (2019)							
CO_2	mmol m^{-2} d^{-1}	763±126	529–1818	841±132	541–1640	739±312	396.5–2251
CH_4	mmol m^{-2} d^{-1}	0.03±0.02	0.01–0.27	0.06±0.03	0.01–0.28	0.09±0.07	0.04–0.57
N_2O	μmol m^{-2} d^{-1}	200±34	119.7–478	249±41	166.5–502	249±107	123.2–674

diffusion of the gas in water (Jähne et al. 1987). Air–water greenhouse gas vertical fluxes ($f_{a/w}$) were estimated from:

$$f_{a/w} = k\alpha(G_w - G_a), \quad (1)$$

where k is the gas transfer velocity coefficient (m d^{-1}), α is the solubility coefficient for the specific gas (Weiss and Price 1980), G_w is the concentration of the gas in a water sample, and G_{atm} is the equilibrium gas concentration for that temperature, conductivity, and pressure. CO_2-eq emissions were computed over 20- and 100-yr sustained global warming potentials to determine the relative importance of each gas and compare it to IPCC estimates, following Neubauer and Megonigal (2019).

Results

Our observations spanned a dry summer-to-autumn transition with only 239 mm of rainfall, less than half the long-term average for this time of year in the region. The last 10 d of observations accumulated ∼ 50% of the total rainfall. Two significant rain events (60 mm on 30 March and 40 mm on

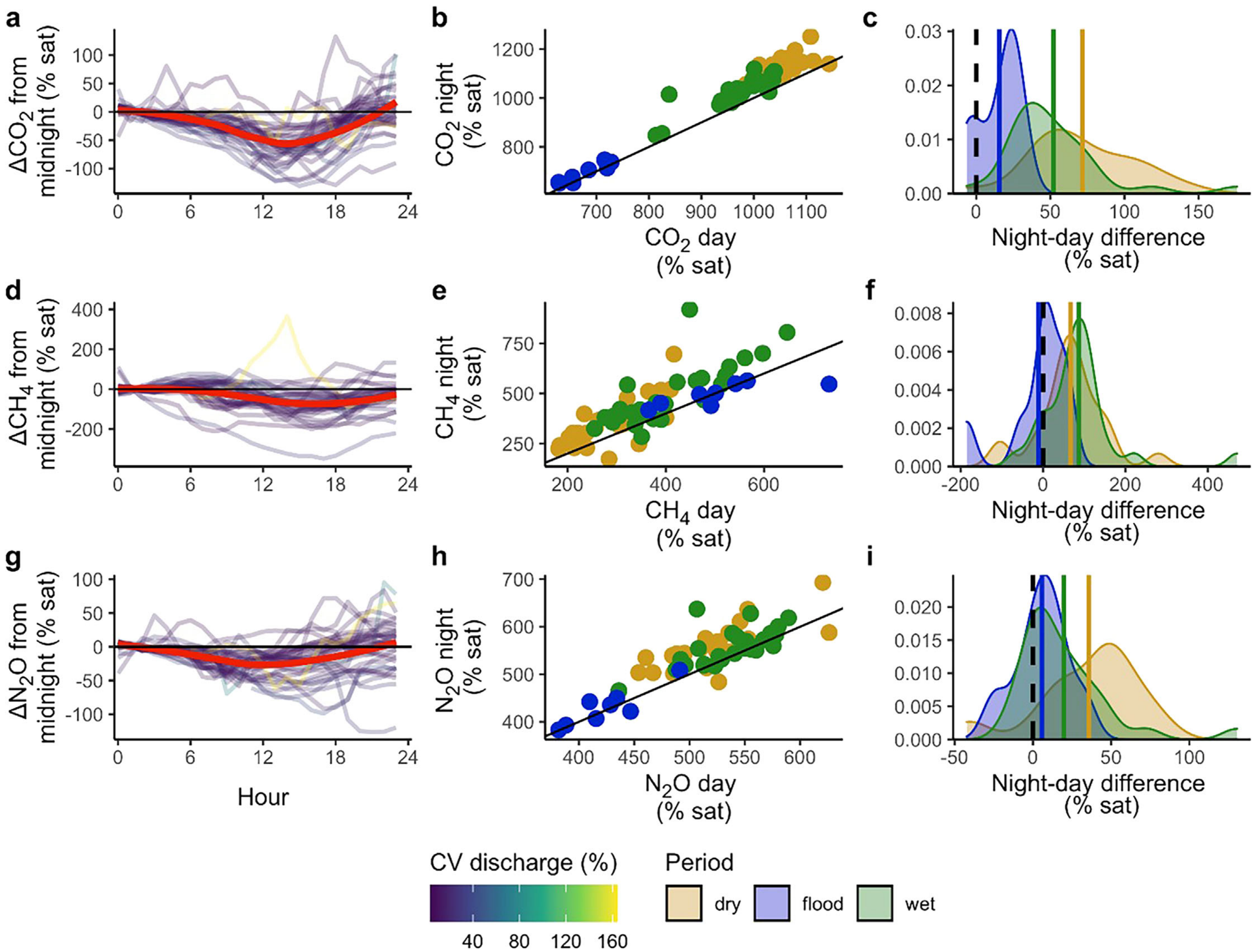

Fig. 2. Day/night comparisons and differences between CO_2, CH_4, and N_2O in Double Crossing Creek, Australia. The first column (plots **a**, **d**, and **g**) is high-resolution 24-h cycles highlighting the within-day variability, using the current velocity of discharge to show that floods can disturb that diel signal. The red lines are averages. CV represents the coefficient of variation of stream discharge (SD/mean) of each day to highlight days when the diel pattern may be altered due to flood events. The second column (plots **b**, **e**, and **h**) is an aggregation of Column 1 data, with the average night and day values for each complete 24 h cycle. Most of the concentrations/fluxes are higher at night. The solid black line is a 1 : 1 ratio. The third column (plots **c**, **f**, and **i**) is an extra step of aggregation, with density plots showing the magnitude of difference from day–night, and across hydrological regimes. The vertical, colored lines show the mean values. Orange, green, and blue shading indicate periods of dry, wet, and flood, respectively.

02 April) increased soil moisture from ~ 30% to ~ 60% and stream discharge (Fig. 1). The median stream discharge was $0.01\ m^3\ s^{-1}$ (0.05 quantile = $0.002\ m^3\ s^{-1}$, 0.95 quantile = $0.05\ m^3\ s^{-1}$) with peaks in flow following rain events > 30 mm. Water temperature ranged from 19.2°C to 24.2°C (21.9 ± 0.9°C; mean ± standard deviation). DO was consistently undersaturated at 70.0% ± 5.9%. The pH (7.0 ± 0.08) and specific conductivity (487 ± 11.5 $\mu S\ cm^{-1}$) values were within the range often found for these regional streams. ^{222}Rn ranged from 199 to 587 dpm L^{-1} (392 ± 54 dpm L^{-1}). DOC, NO_3^-, and NH_4^- concentrations ranged from 64 to 447 $\mu mol\ L^{-1}$ (107 ± 77 $\mu mol\ L^{-1}$), 95 to 485 $\mu mol\ L^{-1}$ (180 ± 92 $\mu mol\ L^{-1}$), and 0 to 4.1 $\mu mol\ L^{-1}$ (0.3 ± 0.6 $\mu mol\ L^{-1}$), respectively.

The stream was always a greenhouse gas source to the atmosphere with CO_2, CH_4, and N_2O saturations ranging between 614% and 1290% (984% ± 145%), 169% and 1176% (413% ± 147%), and 361% and 729% (523% ± 60%), respectively (Fig. 1). Using transfer velocities from Raymond et al. (2012), CO_2, CH_4, and N_2O emissions ranged between 201 and 3153 mmol $m^{-2}\ d^{-1}$ (580 ± 231 mmol $m^{-2}\ d^{-1}$), 0 and 0.7 mmol $m^{-2}\ d^{-1}$ (0.04 ± 0.05 mmol $m^{-2}\ d^{-1}$), and 47 and 862 $\mu mol\ m^{-2}\ d^{-1}$ (170 ± 79 $\mu mol\ m^{-2}\ d^{-1}$), respectively. Greenhouse gas emissions using the transfer velocities of Li et al. (2019) were, on average, 30% higher than when using Raymond et al. (2012) (Table 1). All transfer velocities and emissions values reported herein are derived from Raymond et al. (2012). Comparisons from Li et al. (2021) are included in tables and Supporting Information Material.

Observations were grouped into three hydrological periods (Fig. 1; Table 1). Dry conditions represented the first 24 d of sampling (February), accumulating 33 mm of rainfall and a mean runoff of 0.02 ± 0.02 mm d^{-1}. Relatively wet conditions occurred in the following 28 d in March, with 104 mm rainfall and multiple events < 25 mm (mean runoff 0.1 ± 0.08 mm d^{-1}). Flood represented the last 10 d of sampling with 102 mm rainfall and rain events ≥ 40 mm (mean runoff 0.3 ± 0.2 mm d^{-1}). During the flood, the stream's peak discharge increased by one order of magnitude, and depth increased from 4 to 31 cm, overtopping the bank by 1.4 m. Mean CO_2 and N_2O saturations reduced during flood while mean CH_4 saturation increased (Fig. 1) and transfer velocities increased by ~ 160% (Table 1). Runoff from these rainfall events described and captured herein

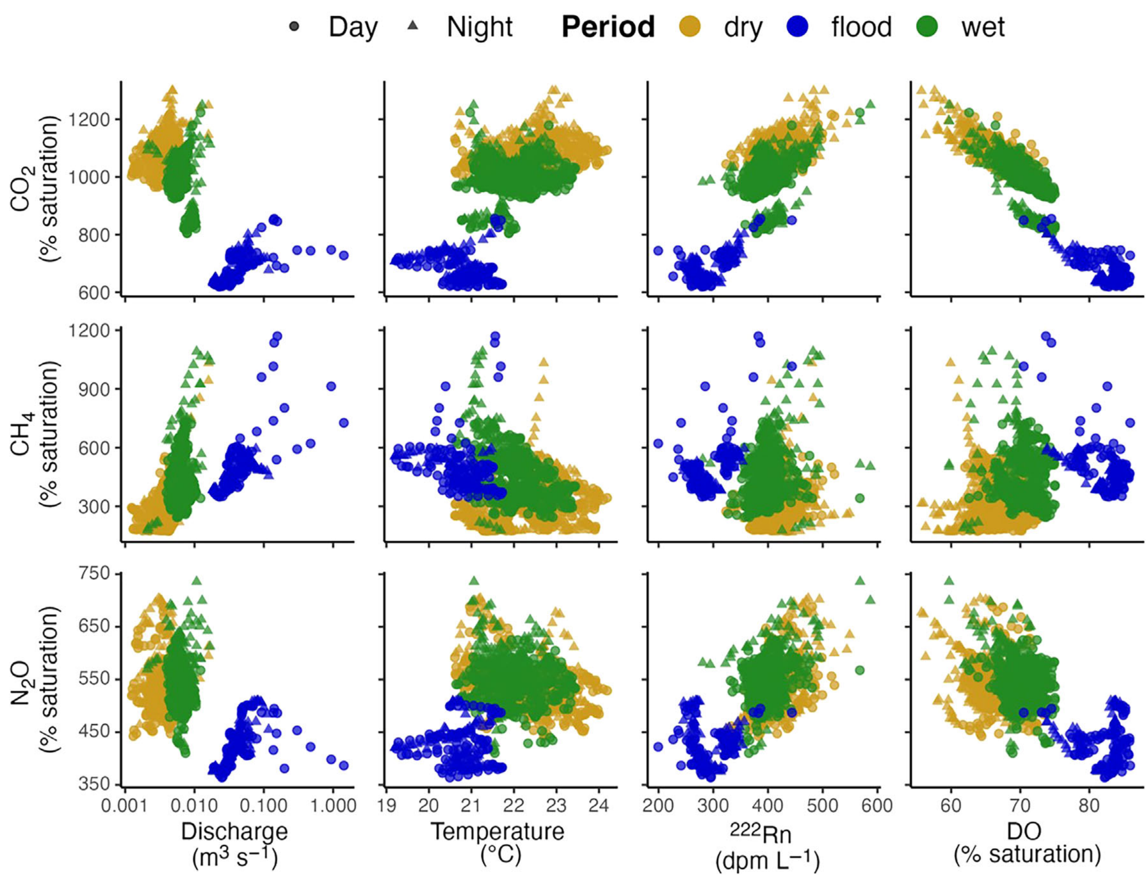

Fig. 3. Scatterplots of drivers of greenhouse gas production over differing hydrological conditions in the day and the night in Double Crossing Creek, NSW, Australia. Circles represent samples collected at night between 00:00 h and 05:00 h, while triangles represent samples collected in the day from 12:00 h to 17:00 h. Orange, green, and blue shading indicate periods of dry, wet, and flood, respectively.

also increased catchment nutrient inputs into the stream (White et al. 2021*a*). Failing to capture the flood would underestimate overall emissions by 6%, 28%, and 10% for CO_2, CH_4, and N_2O.

Stream CO_2, CH_4, and N_2O saturations and emissions varied over diel cycles, with a clear pattern of greater values during the night (Figs. 2, 3). Diel cycles were most pronounced during dry conditions, and dry period parameter changes are reported herein to highlight extremes (*see* Supporting Information Fig. S1; Supporting Information Table S1 for additional day–night comparisons). Lower temperature and DO occurred at night. Mean stream discharge increased from 0.003 ± 0.001 to 0.0045 ± 0.001 $m^3\ s^{-1}$ during the night, reflecting increases in stream current velocity and depths. Radon (a natural groundwater tracer) also experienced diel cycles with nocturnal values $\sim 10\%$ greater than daytime values, implying enhanced nighttime groundwater inputs. Nocturnal mean CO_2, CH_4, and N_2O emissions were 49%, 109%, and 50% higher than daytime emissions. Daytime runoff during the flood period reduced overall diel differences, with mean nocturnal emissions encompassing all hydrological periods 31%, 68%, and 32% greater than daytime for CO_2, CH_4, and N_2O, respectively. Neglecting flood events and nocturnal emissions underestimates overall emissions by 19%, 41%, and 21% for CO_2, CH_4, and N_2O, respectively.

Discussion

Drivers of enhanced nocturnal greenhouse gas emissions

We show enhanced greenhouse gas nocturnal concentrations and emissions of under varying hydrological conditions in a headwater stream. Gómez-Gener et al. (2021) reported a $\sim 30\%$ increase in nighttime CO_2 from a global compilation of high-frequency observations. Here, we highlight potential drivers of CH_4 and N_2O diel variation in a subtropical stream across contrasting hydrological conditions. Instream production, anthropogenic or natural inputs, groundwater inputs, discharge, stream depth, slope, and temperature can all influence greenhouse gas emissions (Raymond et al. 2012). Higher greenhouse gas concentrations and emissions are often found in lower order compared to higher Strahler order streams (Li et al. 2021), reflecting higher connectivity to terrestrial ecosystems.

The higher nocturnal greenhouse gas emissions in this stream observed during the dry and transition to relatively wet periods were explained by greater gas transfer velocities (14–32%) and greenhouse gas saturations (3–26%) at night (Supporting Information Table S1). The elevation in nocturnal gas transfer velocities reflected changes in depth (6% and 21% higher at night) and current velocity (13% and 24% higher at night) (Supporting Information Fig. S3). The diel variation was most pronounced during the dry period in February when the 10% increase in ^{222}Rn indicates greater nighttime groundwater inputs. The diel variation was intensified by the higher ^{222}Rn concentrations during baseflow (Fig. 3), indicating a higher ratio of groundwater input relative to overall flows (Kaule and Gilfedder 2021) that enhances CO_2, CH_4, and N_2O saturations (Fig. 3). The groundwater contribution became less evident in terms of diel cycles of greenhouse gases and radon as flows through surficial soil horizons made a greater contribution in the flood period.

Enhanced nocturnal CO_2 production is typically explained by the cessation of photosynthesis at night (Attermeyer et al. 2021; Gómez-Gener et al. 2021). In this stream, the short residence time and large groundwater inputs may minimize instream respiration as the key driver (Hotchkiss et al. 2015), even if the high C and N inputs (White et al. 2021*a*) can fuel metabolic processes. Rather, the sustained stream greenhouse gas supersaturation was likely due to the gas export from soil respiration through shallow groundwater pathways (Lupon et al. 2019). Groundwater inputs are also higher at night, as revealed by consistently higher ^{222}Rn concentrations and stream discharge. Taken together, higher nighttime groundwater contributions, higher water flows, and higher gas transfer velocities create a multiplicative effect, enhancing emissions to the atmosphere at night.

Oxygen availability is a major driver of instream greenhouse gas production (Wu et al. 2018). Lotic N_2O concentrations are expected to be higher at night when DO is generally lower (Rosamond et al. 2012). In agriculturally impacted streams, denitrification and related N_2O production are stimulated under low DO and high NO_3^- conditions (Rosamond et al. 2012; Liu et al. 2017). Concentrations of DOC and NO_3^- were overall high and increased with discharge due to high anthropogenic loading from surrounding horticultural activities (Wadnerkar et al. 2021; White et al. 2021*a*). Both DOC and NO_3^- exports may contribute to increased emissions, reflecting a correlation between both the export of DOC and NO_3^- and the export of CO_2 and N_2O from soil respiration, which accumulates in the biochemically reactive surface area of pore waters and is exported when discharge increases (Marzadri et al. 2017). Here, DO saturations were 10% lower during the night during dry and negatively correlated with N_2O saturations (Fig. 3; Supporting Information Figs. S3, S4). Our observations of increased nocturnal N_2O coupled with low DO and high NO_3^- are consistent with observations of diel cycling in agricultural catchments in China (Wu et al. 2018), the United States (Laursen and Seitzinger 2004), Canada (Rosamond et al. 2011), and in larger rivers (Huang et al. 2013). In this stream, N_2O emissions increased with discharge and directly after the second major rainfall event, consistent with the highest NO_3^- and reducing N_2O concentrations as expected for regional agricultural streams (Andrews et al. 2021).

In contrast to N_2O, CH_4 emissions found here were at the lower end of global ranges (Rosentreter et al. 2021; Stanley et al. 2023). As a comparison, the highest CH_4 emissions in our study (0.7 mmol $m^{-2}\ d^{-1}$) were one order of magnitude lower than temperate agricultural headwaters (Schade et al. 2016) and negligible in comparison to temperate peatland headwaters (Taillardat et al. 2022). These low CH_4 emissions are expected with oxygen and NO_3^- acting as preferential terminal electron

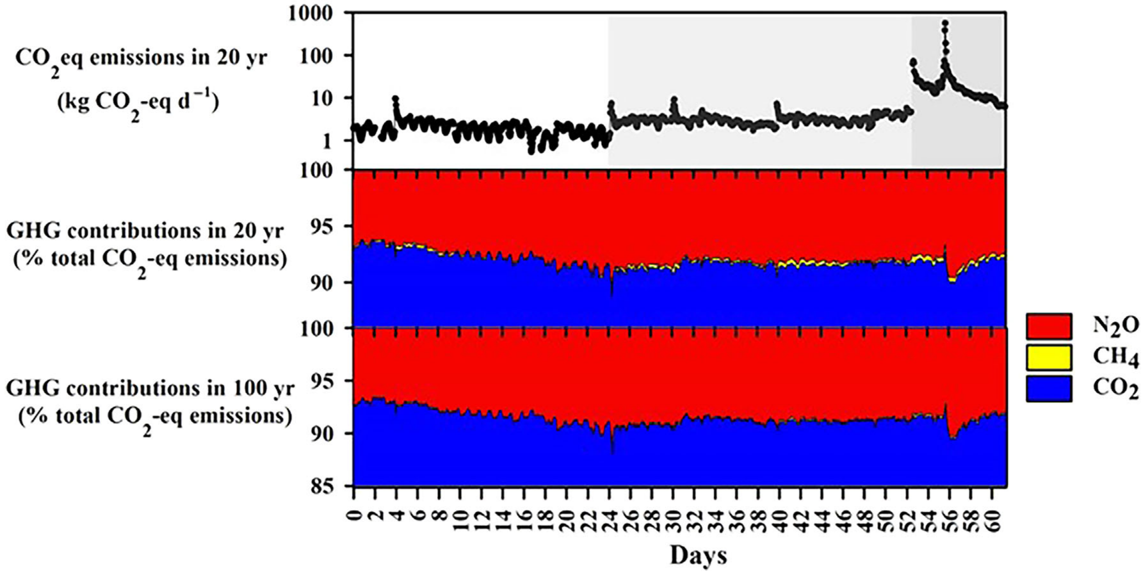

Fig. 4. CO_2-equivalent (CO_2-eq) emissions on a 20-yr SGWP timescale over the 62-day time series observation period in Double Crossing Creek, NSW, Australia. White, light gray, and dark gray shading indicate periods of dry, wet, and flood, respectively. Percentage contributions to total emissions over 20- and 100-yr timescales for CO_2, CH_4, and N_2O (Neubauer and Megonigal 2019).

acceptors, inhibiting methanogenesis. Low CH_4 emissions have been observed in agriculturally impacted headwater streams with high DOC and high NO_3^- (Schade et al. 2016) due to denitrifying bacteria outcompeting methanogens for organic substrates (McCrackin and Elser 2011; Bodelier and Steenbergh 2014). The higher concentration of N_2O, coupled with lower CH_4 observed over the dry period (Fig. 3), also suggests that denitrifiers outcompete methanogens. Other potential loss pathways may be some instream oxidation of CH_4, with estimates suggesting that half of the dissolved CH_4 in supersaturated lowland headwater streams in the United States is oxidized to CO_2 before evasion (Robison et al. 2022).

Groundwater is an important driver of river CH_4 emissions (Lupon et al. 2019; Rocher-Ros et al. 2023). Overall saturations of CO_2 and N_2O were consistent with ^{222}Rn and diluted as flow increased. The inverse relationship with discharge suggests that lateral groundwater was the dominant source of CO_2 and N_2O. However, CH_4, while saturated in the stream, had no relationship with ^{222}Rn and an overall positive correlation with discharge (Fig. 3; Supporting Information Fig. S4). CH_4 in regional streams increases with catchment forest cover during intense runoff periods (Andrews et al. 2021). Hence, we suspect CH_4 sources from upstream forests under high runoff following rainfall, widening the catchment area where methanogenesis may occur.

Implications

Anthropogenic emissions of CO_2, CH_4, and N_2O contribute to 76%, 16%, and 6% of global warming potentials, respectively (IPCC 2022). Translating stream emissions to warming potential, we found that CO_2, CH_4, and N_2O contributed 92.7%, 0.2%, and 7.1% of total aquatic CO_2-eq emissions (Fig. 4). Overall, average stream N_2O and CO_2 emissions were $\sim$ 22% and $\sim$ 19% higher than their anthropogenic global mean contributions, and CH_4 was negligible. Our findings on low CH_4 emissions contribute to the emerging literature on stream CH_4 dynamics (Stanley et al. 2016; Li et al. 2021; Rosentreter et al. 2021). Our CO_2-eq 20- and 100-yr potential emissions show important variations in N_2O between dry and flood periods.

Default emissions factors (EFs) have been established by the IPCC for waterways that contribute to indirect N_2O emissions via leaching and runoff (EF_{5r}). The ratio of dissolved N_2O concentration to dissolved inorganic nitrogen concentration (EF) was used to calculate an in situ EF (Hu et al. 2016). We employ the modified default EF_{5r} emission factor (0.0075 ± 0.025–0.0005 kg N_2O kg^{-1}) to compare our observations to the IPCC indirect emissions model (Hergoualc'h et al. 2019). We found an in situ EF of 0.0003 over the observation period, well below the IPCC default EF_{5r} emission factor. Our estimate capturing day–night cycles and hydrological extremes is at the lower end of a compilation of 52 studies in modified waterways, revealing EFs ranging from 0.00005 to 0.1133 (Webb et al. 2021) and consistent with summer values found in agricultural headwaters in the United Kingdom (Hama-Aziz et al. 2017). Agriculturally impacted streams in Canada had EFs of 0.0044 at night and 0.0034 in the day (Baulch et al. 2012), consistent with our observations.

Despite our inclusion of higher nighttime and flood-time measurements, the emissions observed in this study are still relatively low when compared with results from other sites often sampled during the day only. A wide range of CO_2 (Gómez-Gener et al. 2021), CH_4 (Stanley et al. 2023), and N_2O (Maavara et al. 2019) emissions have been observed in streams with different climatic and geomorphological conditions. For example, high latitude streams subject to wintertime freezing, spring thaw, and major seasonal variability in daylight hours (Rocher-Ros et al. 2023) will likely have diel CH_4 and N_2O cycles that contrast to our subtropical stream with minor seasonal variability. Regardless, albeit at high latitudes, the nights during summer are short or inexistent; the change in intensity from day to night is sufficient to cause large diel changes in O_2 and CO_2 owing to photosynthesis (Rocher-Ros et al. 2020). While high-resolution observations of CO_2 have been performed in high-latitude streams (Gómez-Gener et al. 2021), we are unaware of detailed time series observations of CH_4 and N_2O in cold temperate or polar streams. Hence, additional time series observations capturing day–night and seasonal cycles are needed in multiple streams with different land use, climate, and geomorphology.

Conclusions

Our analysis has implications for global estimates of greenhouse gas emissions from headwater streams. Global estimates of riverine CO_2, CH_4, and N_2O emissions exhibit high spatial and temporal variability and are largely based on discrete sampling during the day (Marzadri et al. 2021; Liu et al. 2022; Rocher-Ros et al. 2023), potentially missing higher emissions that occur during the night and floods. In our study, not only were CO_2 emissions 31% higher at night in line with global averages (Gómez-Gener et al. 2021), but CH_4 (68%) and N_2O (32%) emissions were also higher at night. Even though our results are from a single stream, the consistent patterns and the drivers suggest that those mechanisms may be prevalent across other headwater streams around the globe. Therefore, global estimates of riverine CH_4 and N_2O emissions are likely underestimated for overlooking enhanced emissions during the night and during floods.

References

Andrews, L. F., P. D. Wadnerkar, S. A. White, X. Chen, R. E. Correa, L. C. Jeffrey, and I. R. Santos. 2021. Hydrological, geochemical and land use drivers of greenhouse gas dynamics in eleven sub-tropical streams. Aquat. Sci. **83**: 40. doi:10.1007/s00027-021-00791-x

Attermeyer, K., and others. 2021. Carbon dioxide fluxes increase from day to night across European streams. Commun. Earth Environ. **2**: 118. doi:10.1038/s43247-021-00192-w

Australian Government Bureau of Meteorology. 2022. Climate data online. http://www.bom.gov.au/climate/data/

Battin, T. J., and others. 2023. River ecosystem metabolism and carbon biogeochemistry in a changing world. Nature **613**: 449–459. doi:10.1038/s41586-022-05500-8

Baulch, H. M., P. J. Dillon, R. Maranger, J. J. Venkiteswaran, H. F. Wilson, and S. L. Schiff. 2012. Night and day: Short-term variation in nitrogen chemistry and nitrous oxide emissions from streams. Freshw. Biol. **57**: 509–525. doi:10.1111/j.1365-2427.2011.02720.x

Bodelier, P. L. E., and A. K. Steenbergh. 2014. Interactions between methane and the nitrogen cycle in light of climate change. Curr. Opin. Environ. Sustain. **9-10**: 26–36. doi:10.1016/j.cosust.2014.07.004

Clarke, B., F. Otto, R. Stuart-Smith, and L. Harrington. 2022. Extreme weather impacts of climate change: An attribution perspective. Environ. Res. Clim. **1**: 012001. doi:10.1088/2752-5295/ac6e7d

Gómez-Gener, L., and others. 2021. Global carbon dioxide efflux from rivers enhanced by high nocturnal emissions. Nat. Geosci. **14**: 289–294. doi:10.1038/s41561-021-00722-3

Hama-Aziz, Z. Q., K. M. Hiscock, and R. J. Cooper. 2017. Indirect nitrous oxide emission factors for agricultural field drains and headwater streams. Environ. Sci. Technol. **51**: 301–307. doi:10.1021/acs.est.6b05094

Hergoualc'h, K., and others. 2019. *N_2O emissions from managed soils, and CO_2 emissions from lime and urea application*. IPCC.

Hill, A. R. 2019. Groundwater nitrate removal in riparian buffer zones: A review of research progress in the past 20 years. Biogeochemistry **143**: 347–369. doi:10.1007/s10533-019-00566-5

Ho, L., R. Jerves-Cobo, M. Barthel, J. Six, S. Bode, P. Boeckx, and P. Goethals. 2022. Greenhouse gas dynamics in an urbanized river system: Influence of water quality and land use. Environ. Sci. Pollut. Res. **29**: 37277–37290. doi:10.1007/s11356-021-18081-2

Hotchkiss, E. R., R. O. Hall Jr., R. A. Sponseller, D. Butman, J. Klaminder, H. Laudon, M. Rosvall, and J. Karlsson. 2015. Sources of and processes controlling CO_2 emissions change with the size of streams and rivers. Nat. Geosci. **8**: 696–699. doi:10.1038/ngeo2507

Hu, M., D. Chen, and R. A. Dahlgren. 2016. Modeling nitrous oxide emission from rivers: A global assessment. Glob. Change Biol. **22**: 3566–3582. doi:10.1111/gcb.13351

Huang, W.-M., K.-X. Zhu, W. Zhao, B.-S. Yu, X.-G. Yuan, R.-J. Feng, Y.-H. Bi, and Z.-Y. Hu. 2013. Diurnal changes in greenhouse gases at water-air interface of Xiangxi River in autumn and their influencing factors. Huan Jing Ke Xue **34**: 1270–1276.

IPCC. 2022. Climate change 2022: Mitigation of climate change. *In* P. R. Shukla and others [eds.], *Contribution of working group III to the sixth assessment report of the intergovernmental panel on climate change*. Cambridge Univ. Press. doi:10.1017/9781009157926

Jähne, B., G. Heinz, and W. Dietrich. 1987. Measurement of the diffusion coefficients of sparingly soluble gases in water. J. Geophys. Res.: Oceans **92**: 10767–10776. doi:10.1029/JC092iC10p10767

Kaule, R., and B. S. Gilfedder. 2021. Groundwater dominates water fluxes in a headwater catchment during drought. Front. Water **3**: 706932. doi:10.3389/frwa.2021.706932

Laursen, A. E., and S. P. Seitzinger. 2004. Diurnal patterns of denitrification, oxygen consumption and nitrous oxide production in rivers measured at the whole-reach scale. Freshw. Biol. **49**: 1448–1458. doi:10.1111/j.1365-2427.2004.01280.x

Li, S., R. Mao, Y. Ma, and V. V. S. S. Sarma. 2019. Gas transfer velocities of CO_2 in subtropical monsoonal climate streams and small rivers. Biogeosciences **16**: 681–693. doi:10.5194/bg-16-681-2019

Li, M., and others. 2021. Headwater stream ecosystem: An important source of greenhouse gases to the atmosphere. Water Res. **190**: 116738. doi:10.1016/j.watres.2020.116738

Liu, S., and others. 2017. A meta-analysis of fertilizer-induced soil NO and combined NO+N_2O emissions. Glob. Change Biol. **23**: 2520–2532. doi:10.1111/gcb.13485

Liu, S., Q. Gao, J. Wu, Y. Xie, Q. Yang, R. Wang, J. Zhang, and Q. Liu. 2022. Spatial distribution and influencing mechanism of CO_2, N_2O and CH_4 in the Pearl River Estuary in summer. Sci. Total Environ. **846**: 157381. doi:10.1016/j.scitotenv.2022.157381

Lupon, A., B. A. Denfeld, H. Laudon, J. Leach, J. Karlsson, and R. A. Sponseller. 2019. Groundwater inflows control patterns and sources of greenhouse gas emissions from streams. Limnol. Oceanogr. **64**: 1545–1557. doi:10.1002/lno.11134

Maavara, T., R. Lauerwald, G. G. Laruelle, Z. Akbarzadeh, N. J. Bouskill, P. Van Cappellen, and P. Regnier. 2019. Nitrous oxide emissions from inland waters: Are IPCC estimates too high? Glob. Change Biol. **25**: 473–488. doi:10.1111/gcb.14504

Marzadri, A., M. M. Dee, D. Tonina, A. Bellin, and J. L. Tank. 2017. Role of surface and subsurface processes in scaling N_2O emissions along riverine networks. Proc. Natl. Acad. Sci. USA **114**: 4330–4335. doi:10.1073/pnas.1617454114

Marzadri, A., G. Amatulli, D. Tonina, A. Bellin, L. Q. Shen, G. H. Allen, and P. A. Raymond. 2021. Global riverine nitrous oxide emissions: The role of small streams and large rivers. Sci. Total Environ. **776**: 145148. doi:10.1016/j.scitotenv.2021.145148

McCrackin, M. L., and J. J. Elser. 2011. Greenhouse gas dynamics in lakes receiving atmospheric nitrogen deposition: Greenhouse gases in lakes. Glob. Biogeochem. Cycles **25**: GB4005. doi:10.1029/2010GB003897

Neubauer, S. C., and J. P. Megonigal. 2019. Correction to: Moving beyond global warming potentials to quantify the climatic role of ecosystems. Ecosystems **22**: 1931–1932. doi:10.1007/s10021-019-00422-5

Noto, S., F. Tauro, A. Petroselli, C. Apollonio, G. Botter, and S. Grimaldi. 2022. Low-cost stage-camera system for continuous water-level monitoring in ephemeral streams. Hydrol. Sci. J. **67**: 1439–1448. doi:10.1080/02626667.2022.2079415

Odum, H. T. 1956. Primary production in flowing waters. Limnol. Oceanogr. **1**: 102–117. doi:10.4319/lo.1956.1.2.0102

Raymond, P. A., and others. 2012. Scaling the gas transfer velocity and hydraulic geometry in streams and small rivers. Limnol. Oceanogr.: Fluids Environ. **2**: 41–53. doi:10.1215/21573689-1597669

Robison, A. L., W. M. Wollheim, C. R. Perryman, A. R. Cotter, J. E. Mackay, R. K. Varner, P. Clarizia, and J. G. Ernakovich. 2022. Dominance of diffusive methane emissions from lowland headwater streams promotes oxidation and isotopic enrichment. Front. Environ. Sci. **9**: 791305. doi:10.3389/fenvs.2021.791305

Rocher-Ros, G., R. A. Sponseller, A.-K. Bergström, M. Myrstener, and R. Giesler. 2020. Stream metabolism controls diel patterns and evasion of CO_2 in Arctic streams. Glob. Change Biol. **26**: 1400–1413. doi:10.1111/gcb.14895

Rocher-Ros, G., E. H. Stanley, L. C. Loken, N. J. Casson, P. A. Raymond, S. Liu, G. Amatulli, and R. A. Sponseller. 2023. Global methane emissions from rivers and streams. Nature **621**: 530–535. doi:10.1038/s41586-023-06344-6

Rosamond, M. S., S. J. Thuss, S. L. Schiff, and R. J. Elgood. 2011. Coupled cycles of dissolved oxygen and nitrous oxide in rivers along a trophic gradient in southern Ontario, Canada. J. Environ. Qual. **40**: 256–270. doi:10.2134/jeq2010.0009

Rosamond, M. S., S. J. Thuss, and S. L. Schiff. 2012. Dependence of riverine nitrous oxide emissions on dissolved oxygen levels. Nat. Geosci. **5**: 715–718. doi:10.1038/ngeo1556

Rosentreter, J. A., and others. 2021. Half of global methane emissions come from highly variable aquatic ecosystem sources. Nat. Geosci. **14**: 225–230. doi:10.1038/s41561-021-00715-2

Schade, J. D., J. Bailio, and W. H. McDowell. 2016. Greenhouse gas flux from headwater streams in New Hampshire, USA: Patterns and drivers: Greenhouse gas flux from headwater streams. Limnol. Oceanogr. **61**: S165–S174. doi:10.1002/lno.10337

Siedler, G., and H. Peters. 1986. Properties of sea water, physical properties (general), p. 233–264. *In* J. Sündermann [ed.], *LANDOLT-BÖRNSTEIN, Numerical data and functional relationships in science and technology*, v. **3a**. Springer, https://oceanrep.geomar.de/id/eprint/20134/

Stanley, E. H., N. J. Casson, S. T. Christel, J. T. Crawford, L. C. Loken, and S. K. Oliver. 2016. The ecology of methane in streams and rivers: Patterns, controls, and global significance. Ecol. Monogr. **86**: 146–171. doi:10.1890/15-1027

Stanley, E. H., L. C. Loken, N. J. Casson, S. K. Oliver, R. A. Sponseller, M. B. Wallin, L. Zhang, and G. Rocher-Ros.

2023. GRiMeDB: The Global River methane database of concentrations and fluxes. Earth Syst. Sci. Data **15**: 2879–2926. doi:10.5194/essd-15-2879-2023

Taillardat, P., and others. 2022. Carbon dioxide and methane dynamics in a peatland headwater stream: Origins, processes and implications. J. Geophys. Res.: Biogeosci. **127**: e2022JG006855. doi:10.1029/2022JG006855

Wadnerkar, P. D., and others. 2021. Land use and episodic rainfall as drivers of nitrogen exports in subtropical rivers: Insights from $\delta^{15}N\text{-}NO_3^-$, $\delta^{18}O\text{-}NO_3^-$ and ^{222}Rn. Sci. Total Environ. **758**: 143669. doi:10.1016/j.scitotenv.2020.143669

Webb, J. R., T. J. Clough, and W. C. Quayle. 2021. A review of indirect N_2O emission factors from artificial agricultural waters. Environ. Res. Lett. **16**: 043005. doi:10.1088/1748-9326/abed00

Weiss, R. F., and B. A. Price. 1980. Nitrous oxide solubility in water and seawater. Mar. Chem. **8**: 347–359. doi:10.1016/0304-4203(80)90024-9

White, S. A., and others. 2021*a*. Natural attenuation of large anthropogenic nitrate loads in a subtropical stream revealed by $\delta^{15}N$ and $\delta^{18}O$. J. Hydrol. **598**: 126077. doi:10.1016/j.jhydrol.2021.126077

White, S. A., I. R. Santos, S. R. Conrad, C. J. Sanders, and S. Hessey. 2021*b*. Large aquatic nitrous oxide emissions downstream of intensive horticulture driven by rain events. J. Hydrol. **596**: 126066. doi:10.1016/j.jhydrol.2021.126066

Woodrow, R. L., and S. A. White. 2023. Enhanced stream greenhouse gas emissions at night and during flood events. figshare. doi:10.6084/m9.figshare.24439210.v1

Woodrow, R. L., and others. 2022. Nitrous oxide hot moments and cold spots in a subtropical estuary: Floods and mangroves. Estuar. Coast. Shelf Sci. **264**: 107656. doi:10.1016/j.ecss.2021.107656

Wu, S., J. Chen, C. Li, D. Kong, K. Yu, S. Liu, and J. Zou. 2018. Diel and seasonal nitrous oxide fluxes determined by floating chamber and gas transfer equation methods in agricultural irrigation watersheds in southeast China. Environ. Monit. Assess. **190**: 122. doi:10.1007/s10661-018-6502-0

Yao, Y., H. Tian, H. Shi, S. Pan, R. Xu, N. Pan, and J. G. Canadell. 2019. Increased global nitrous oxide emissions from streams and rivers in the Anthropocene. Nat. Clim. Change **10**: 138–142. doi:10.1038/s41558-019-0665-8

Acknowledgments

This project was partially funded by the Coffs Harbour City Council's Environmental Levy program and the Australian Research Council (FT170100327 and LE170100007) and is part of RW's PhD Thesis. Open access publishing facilitated by Southern Cross University, as part of the Wiley - Southern Cross University agreement via the Council of Australian University Librarians.

Submitted 05 March 2023
Revised 20 December 2023
Accepted 08 January 2024